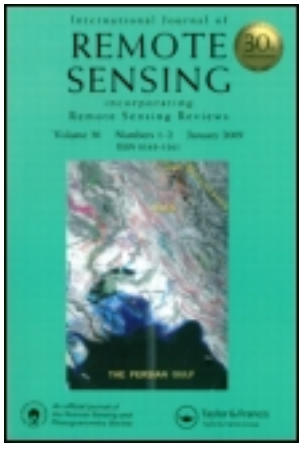

International Journal of Remote Sensing

Publication details, including instructions for authors and subscription information:
http://www.tandfonline.com/loi/tres20

The effect of soil moisture and wind speed on aerosol optical thickness retrieval in a desert environment using SEVIRI thermal channels

Sagar Prasad Parajuli [a], Imen Gherboudj [a] & Hosni Ghedira [a]

[a] Earth Observation and Hydro-Climatology Lab, Masdar Institute of Science and Technology, Masdar City, Abu Dhabi, UAE

Published online: 11 Apr 2013.

To cite this article: Sagar Prasad Parajuli, Imen Gherboudj & Hosni Ghedira (2013) The effect of soil moisture and wind speed on aerosol optical thickness retrieval in a desert environment using SEVIRI thermal channels, International Journal of Remote Sensing, 34:14, 5054-5071, DOI: 10.1080/01431161.2013.788262

To link to this article: http://dx.doi.org/10.1080/01431161.2013.788262

International Journal of Remote Sensing, 2013
Vol. 34, No. 14, 5054–5071, http://dx.doi.org/10.1080/01431161.2013.788262

Taylor & Francis
Taylor & Francis Group

The effect of soil moisture and wind speed on aerosol optical thickness retrieval in a desert environment using SEVIRI thermal channels

Sagar Prasad Parajuli, Imen Gherboudj, and Hosni Ghedira*

Earth Observation and Hydro-Climatology Lab, Masdar Institute of Science and Technology, Masdar City, Abu Dhabi, UAE

(*Received 22 August 2012; accepted 26 November 2012*)

Dust emission and deposition are associated with several factors such as surface roughness, land cover, soil properties, soil moisture (SM), and wind speed (WS). A combination of land surface and remote-sensing models has recently been investigated for dust detection and monitoring. The thermal bands of the Meteosat Second Generation Spinning Enhanced Visible and Infrared Imager (MSG/SEVIRI) satellite are widely used for qualitative detection of dust over desert because of their high spectral and temporal resolutions. In this work, the contribution of ground-measured WS data and satellite-measured SM data on aerosol optical thickness (AOT) retrieval was investigated using an artificial neural network (ANN) model. ANNs have been applied in similar applications and have shown a higher performance than simple multiple-regression models. This performance is mainly due to the ANN's ability to capture complex and non-linear relationships between inputs and outputs. A combination of MSG/SEVIRI brightness temperature (BT)/brightness temperature differences (BTDs), $BTD_{3.9–10.8}$, $BTD_{8.7–10.8,}$ $BTD_{10.8–12}$, and $BT_{3.9}$, was used as input to the base ANN model while Aerosol Robotic Network (AERONET) AOT (level 2) data at 0.5 μm were used as output. These input/output sets were obtained from two stations (Hamim and Mezaira) lying in the inland desert of the United Arab Emirates (UAE). About 3800 observations were collected, of which two-thirds were used to train the ANN model and the remaining third was kept as an independent set to assess the accuracy of the trained model. Later, Advanced Microwave Scanning Radiometer Earth Observing System (AMSR-E) SM data and ground-measured WS data were used as additional inputs to the base model to investigate their contribution to the AOT retrieval. SM data consist of daytime AMSR-E-derived daily and collected from a National Snow and Ice Data Centre (NSIDC)-archived database. Hourly average WS data were also collected at 10 m height in the same AERONET sites from two stations managed by the UAE National Centre of Meteorology and Seismology. All ground and satellite measurements were extracted for the closest time to AERONET measurements. The use of these additional inputs has been shown to have a positive impact on the accuracy of simulated AOT. The addition of these inputs to the base ANN increased R^2 from 0.68 to 0.76 and reduced root mean square error from 0.113 to 0.09.

1. Introduction

Dust and sandstorms are common phenomena in desert and arid environments. Both create potentially hazardous air quality and adversely affect climate at both regional and worldwide scales (Sokolik and Toon 1996). The frequent occurrence of dust storms has a direct

*Corresponding author. Email: hghedira@masdar.ac.ae

effect on human health, the economy, and the environment, making its detection and assessment of utmost importance. Dust emission and deposition are associated with the transport of human diseases, plant nutrition, and crop diseases (Kellogg and Griffin 2006). Their frequent occurrence has also been found to have a direct effect on accelerating the corrosion of historical buildings and monuments (Varotsos, Tzanis, and Cracknell 2009). Additionally, the presence of dust aerosols has a major impact on the performance of solar energy systems by attenuating the incident solar irradiance and through deposition on solar collectors (Eissa, Chiesa, and Ghedira 2012).

Spaceborne remote sensing can allow dust monitoring as it can provide long-term and global observations. The visible and thermal infrared (TIR) channels of different sensors such as the Total Ozone Mapping Spectrometer (TOMS), Moderate Resolution Imaging Spectroradiometer (MODIS), and MSG/Spinning Enhanced Visible and Infrared Imager (SEVIRI) have been widely used for dust detection and monitoring (Prospero et al. 2002; Zhang et al. 2006; Schepanski et al. 2007). These applications were built on the basis of the strong dependency of scattered and absorbed solar radiation on dust layer properties, i.e. aerosol concentration, particle size distribution, and height (Ackerman 1989; Ackerman 1997; Li et al. 2007). It has been shown through several studies that the techniques using thermal bands have a distinct advantage over visible bands for detecting dust over bright underlying surfaces, such as desert, and during the night (Ackerman 1989; Legrand et al. 1989; Zhang et al. 2006). Thus, several methods based on brightness temperature (BT) in thermal bands (i.e. $BT_{3.7}$, $BT_{10.8}$, and BT_{11}, where the subscripts represent wavelengths in μm) have been proposed for qualitative monitoring of dust (Legrand, Fattori, and N'doume 2001; Schepanski et al. 2007). Other methods derive dust indices or aerosol optical thickness (AOT), which expresses the fraction of radiation passing through a dust layer for quantitative monitoring of dust in the atmosphere (Hsu et al. 2004; Zhang et al. 2006; Li et al. 2007; Jolivet et al. 2008; Brindley and Russell 2009; Paepe and Dewitte 2009). Ground-based measurements collected by the Aerosol Robotic Network (AERONET) or European Aerosol Research Lidar Network (EARLINET) are widely used as truth data in such developments. However, the quantitative monitoring of dust over land is complex for two main reasons. First, the dust has a short lifetime resulting in a high spatial and temporal variability of its physical characteristics (concentration, particle size distribution, and chemical composition). Secondly, dust emission depends upon a number of land surface properties such as wind speed (WS), soil moisture (SM), vegetation, and sediment (Ginoux et al. 2001; Prospero et al. 2002; Shao 2008).

The influence of WS and SM on satellite-derived dust emission techniques has not been undertaken to date. Artificial neural network (ANN) techniques can be used to assess the contribution of these two parameters to BTs in aerosol retrieval. ANNs can model complex real-world problems provided key variables affecting the system under consideration are identified (Wong 1991; Zhang, Patuwo, and Hu 1998). ANNs have been widely used in different remote-sensing-related applications thanks to their non-parametric nature and their relatively easy adaptation to different data types and formats (Wong 1991; Paola and Schowengerdt 1995; Zhang, Patuwo, and Hu 1998). The use of ANNs in remote-sensing applications has been increasing rapidly over the past three decades as the quality and quantity of remotely sensed and ground measurement data sets are also increasing.

The available wind data are either measured locally from meteorological stations or predicted by weather forecast modelling at the global scale, such as ERA-Interim data (Simmons et al. 2007). Unlike meteorological data, the accuracy of predicted wind data from the weather forecast is more accurate at a global scale but less accurate at a local scale, as they are usually reported as coarse-gridded data. A network of stations with wider geographic coverage can be used to derive WS data at an unknown point using statistical

methods. WM is generally measured at 10 m height in weather stations. However, in many dust emission models, effective WS at the ground surface (wind friction velocity) is used to characterize the dust emission mechanism.

The remotely sensed SM is currently available in coarser resolution of about 25 km from several passive microwave satellites such as the Advanced Microwave Scanning Radiometer Earth Observing System (AMSR-E) and Soil Moisture and Ocean Salinity (SMOS), which were launched in 2002 and 2009, respectively (Kerr et al. 2001; Njoku et al. 2003). The launch of the Soil Moisture Active and Passive (SMAP) satellite, scheduled for 2014–2015, will provide SM measurements at finer resolution (Entekhabi 2010).

The main objectives of this work are (1) to develop an ANN-based model to derive AOT from SEVIRI thermal channels, and (2) to understand and quantify the effect of the main ground parameters affecting dust emission, which are SM and WS. A set of SEVIRI brightness temperature (BT)/brightness temperature difference (BTDs) ($BTD_{3.9–10.8}$, $BTD_{8.7–10.8}$, $BTD_{10.8–12}$, and $BT_{3.9}$) are used as inputs in the base neural network model using AERONET AOT (level 2) data as output. A large data set of about 3800 observations was collected between 2004 and 2010 over two locations lying in the inland desert of the United Arab Emirates (UAE) (Hamim and Mezaira). This data set includes four thermal-infrared bands of SEVIRI at 3 km resolution ($BT_{3.9}$, $BT_{8.7}$, $BT_{10.8}$ and BT_{12}); AMSR-E SM data retrieved from the C- or X-band brightness temperature at 25 km resolution; local WS measured at 10 m height collected from the archive of the UAE National Centre of Meteorology and Seismology (NCMS); and AOT measurements at wavelengths ranging between 0.34 and 1.640 μm obtained from AERONET stations within the study area. Both ground and satellite measurements were extracted for the closest time to AERONET measurements.

2. Background

2.1. Dust emission

WS and SM are the key input parameters of several dust models such as Goddard Chemistry Aerosol Radiation and Transport (GOCART) (Chin et al. 2000; Ginoux et al. 2001), Dust Entrainment and Deposition (DEAD) (Zender, Bian, and Newman 2003), and Global Transport Model of Dust (GMOD) (Yue et al. 2009). Dust emission involves movement of soil particles in both horizontal and vertical directions, commonly known as saltation and suspension, respectively. Saltation is caused by the hopping motion of the coarse sand particles in the horizontal direction and suspension is caused by the direct uplifting of the fine particles by strong wind shear (Shao 2008). When saltating particles strike other small particles, transfer of kinetic energy takes place causing the stationary particles to blow. The forces acting against the wind shear stress are gravity, inter-particle cohesive forces, and capillary forces that are related to the level of moisture in the upper soil layer and soil particle-size distribution. Dust emission takes place when the wind shear stress exceeds the sum of these three forces.

Dust emission is initiated mainly when a dynamic velocity, known as the threshold friction velocity, is reached (Chepil 1956). Several theoretical and empirical relationships relating threshold friction velocity with SM variation have been proposed (Chepil 1956; Bisal and Hsieh 1966; Marticorena and Bergamatti 1995; Selah and Fryrear 1995; Shao and Lu 2000; Wang 2006). Most of these studies were based on the early work of Bagnold (Bagnold 1941), who defined the movement of sand particles in terms of threshold friction velocity. Hence, accurate SM and WS measurements would be of great importance in retrieving dust and sandstorm properties over their originating location. In addition to wind (speed and direction) and SM, other soil and land-cover properties such as soil erodibility,

roughness length, vegetation cover, and soil particle-size distribution are also used in several dust emission models. WS is usually measured at a definite height (e.g. 10 m) and the following logarithmic equation is employed to convert it to surface wind friction velocity (Priestley 1959):

$$u(z) = \frac{u_*}{k} \ln \frac{z}{z_0}, \tag{1}$$

where $u(z)$ is WS at a height z; u_* is wind friction velocity; k is the Von Kármán constant approximated to 0.4; and z_0 is the roughness length which depends upon the median diameter of the soil particles, D_{med}, given by $\frac{D_{\text{med}}}{30}$ (Greeley and Iversen 1985). Equation (1) can be used to derive quantitative estimation of wind friction velocity from WS measured at any height.

2.2. *Remote sensing of dust*

Remote-sensing data have been widely used in dust storm detection and forecasting. Retrieving dust and sandstorm properties over their originating location (i.e. desert, arid, and semi-arid regions) using conventional visible channels is a difficult task because of the bright underlying surfaces (Ackerman 1997). Visible channels can be used to detect dust over dark background such as vegetation and water bodies, because the presence of dust in the atmosphere results in higher reflectance compared with that of dark background. In some cases, heavy dust storms can also be detected over desert using the visible channels when the desert background is sufficiently dark (wet surface) or when the visual properties change due to interaction with atmosphere. However, when the reflectance of the dust is similar to that of underlying desert, it is difficult to detect the presence of dust with visible channels.

To overcome this limitation, several approaches have been proposed using the near-infrared and thermal channels (Shenk and Curran 1974; Ackerman 1989; Legrand et al. 1989; Ackerman 1997; Legrand, Fattori, and N'doume 2001; Zhang et al. 2006; Schepanski et al. 2007; Kluser and Schepanski 2009; Martinez, Ruiz, and Cuevas 2009). Near-infrared and thermal channel radiation decreases during the day in the presence of dust, because the dust layer absorbs more radiation than it emits (Legrand et al. 1989). Ackerman (1997) demonstrated the viability of using brightness temperature difference between bands 3.7 and 11 μm ($BTD_{3.7–11}$) in tracking dust storms by comparing satellite measurements with the observed surface visibility. Another useful approach proposed by Ackerman (1997) and Zhang et al. (2006) is based on the brightness temperature difference between bands 11 and 12 μm ($BTD_{11–12}$). Midday $BTD_{11–12}$ is usually negative in the presence of dust and positive in the case of cloud.

Apart from the qualitative detection of dust mentioned above, thermal bands were also used for the quantitative detection of dust. Quantitative detection consists of deriving the AOT at a specific wavelength from satellite measurements (Hsu et al. 2004; Zhang et al. 2006; Li et al. 2007; Brindley and Russell 2009). Another approach was proposed by Paepe and Dewitte (2009), where AOT at 8.7, 10.8, and 12 μm was derived by establishing a look-up table of emissivity ratios by assuming a clear day to be the day having the maximum value of $BT_{10.8}$ and negative $BTD_{8.7–11}$. Such thresholds of BT/BTD for a clear day have a very dynamic behaviour that depends on environmental and seasonal conditions, making it difficult to agree on a reference clear-sky brightness temperature for each time and location. Other attempts have been made to relate $BT_{10.8}$ with AOT through a linear relationship

(Zhang et al. 2006; Li et al. 2007; Brindley and Russell 2009). These authors showed that $BT_{10.8}/BT_{11}$ is linearly proportional to AOT at 0.55 μm, and $BTD_{10.8–12}/BTD_{11–12}$ is almost linearly proportional to particle size. The visible bands have also been used for retrieving AOT at 0.635 and 0.490 μm (Hsu et al. 2004; Jolivet et al. 2008), but they are less effective over bright reflecting deserts such as those found in the UAE. The Deep Blue algorithm proposed by Hsu et al. (2004) uses the assumption that a desert surface appears darker in the blue channel (0.412 and 0.490 μm). Deep Blue AOT data were retrieved with MODIS sensors available on the Aqua and Terra satellites. However, the low temporal resolution of MODIS data (twice daily) compared with the 15 min resolution of MSG/SEVIRI limits the real-time aspect of the dust detection tool.

2.3. Artificial neural networks

ANNs are commonly used to model complex and non-linear phenomena that involve many variables. Unlike standard statistical tools, ANN models are distribution free and require no prior knowledge of statistical distribution to model a given set of data (Benediktsson, Swain, and Ersoy 1990). However, they require a more intensive iterative computation and their optimization phase is more difficult to understand. The recent significant advances observed in computing speed and data processing technologies have contributed to the increasing expansion of ANNs to several fields of science.

ANNs consist of a set of consecutives layers of neurons: one input layer, one or multiple hidden layer(s), and one output layer. Similar to the biological human neurons, neurons in each layer are connected to all neurons in the adjacent layer(s) but not to neurons of the same layer. The hidden layer(s) lie between the input and output layers and contain the weights and activation functions. Hidden nodes help the ANN model to define a non-linear relationship between inputs and output(s). Without hidden nodes, the model would be equivalent to a linear regression model (Zhang, Patuwo, and Hu 1998). Finding the optimum number of hidden nodes is very important, as too low a number of hidden layers may not be enough to train the data and too many may cause an overfitting of the training data. A commonly used approach is to double the number of input nodes in the hidden layer(s) (Wong 1991).

The values of all connecting weights are computed during the ANN training phase. A back-propagation (BP) method is widely used to train the neural network. Modified algorithms such as the Scaled Conjugate Gradient (SCG) algorithm (Moller 1993) and Kalman filter (KF) (Shah and Palmieri 1990) were found to give varying performance depending upon the nature and format of input/output sets. The SCG training algorithm was used in this study while keeping most of the default training parameters as set in the neural network toolbox of MATLAB (The MathWorks, Inc., Natick, MA, USA). The number of epochs for training is kept to 1000 to optimize the trade-off between training time and model performance. In BP training, the weights given to each connection are adjusted during the training process to minimize the difference between actual output and desired output by evaluating the respective quadratic error, root mean square error (RMSE), absolute error, etc. (Rumelhart, Hinton, and Williams 1986). In the forward pass, the neurons' outputs are updated from the input layer to the output layer to generate the final output; while in the backward pass, the inter-neuron weights assigned in the forward pass are modified backwards starting from the output layer to the input layer (Tso and Mather 2009).

In general, the available data set is divided into three separate sets: training, validation, and testing. A major fraction of the data is utilized for training, since ANN weights are updated based on the training data set. A testing set is necessary to evaluate the performance

of the trained model and is usually kept independent from the training set. A validation set is selected from the training data to avoid overfitting of the ANN by enforcing error criteria.

For the evaluation of the ANN model a regression value (R^2), which gives an indication on how far the simulated outputs are scattered from the actual mean, is calculated. The mean biased error (MBE) and RMSE are used to optimize the ANN architecture and assess the accuracy of the trained model. MBE is the mean of the difference between the target and simulated values. The RMSE is given by the square root of the mean squared error. The RMSE is useful in analysing the results, since it has the same unit as the estimated parameter, which is the AOT in this case.

3. Study site and data analysis

3.1. Study site

Two stations, located at Hamim (22.96°N, 54.3°E) and Mezaira (53.78°E, 23.14°N), were selected in the inland desert region of the UAE (Figure 1). The choice of inland stations helps to minimize the effect of fine-mode pollution (generated by industry and urban areas), as the objective of this study is to analyse wind-eroded dust or coarse-mode dust. In addition, the following aspects were considered during the selection of the two stations.

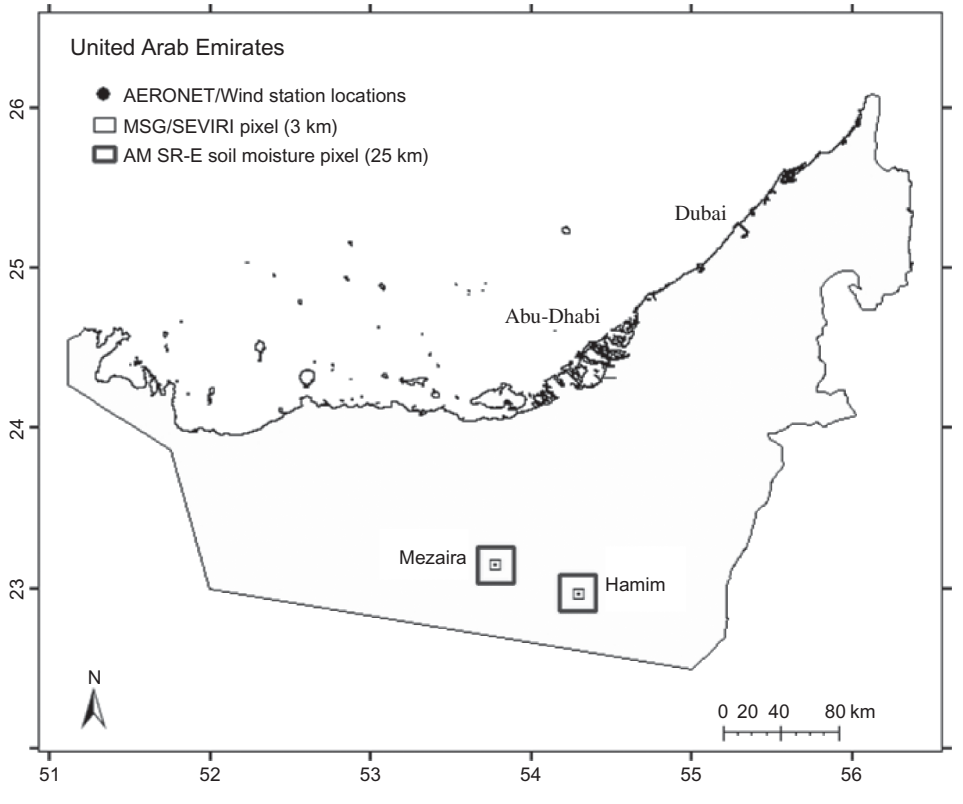

Figure 1. Location of the study sites (Hamim and Mezaira).

- Both stations recorded *in situ* AERONET AOT measurements between 2004 and 2010, managed by the National Aeronautics and Space Administration (NASA).
- Both ground weather stations have carried out meteorological measurements since 1977, managed by the UAE NCMS.

Both stations are located in the same region, which is part of a long stretch of the Empty Quarter desert, extending over Saudi Arabia, UAE, Oman, and Yemen. This region is mainly characterized by low relative humidity, high temperature, and very little annual rainfall (Boer 1997). The soil is dominated by sandy soil (about 95% sand and 5% clay and silt) (EAD 2009). Vegetation in the study area is very sparse and the area is scarcely affected by human activity.

All ground measurements were collected for the period 2004–2010, this being limited mainly by the availability of AERONET data at both stations. The data consist of both ground-based measurements from AERONET and meteorological stations and satellite data from the AMSR-E and the MSG/SEVIRI.

3.2. Data set description

3.2.1. AERONET measurements

AERONET is a global network of ground-based stations measuring different aerosol-related parameters at high temporal resolution (Holben et al. 1998). For this study, level 2 AERONET data were used, as these are cloud filtered and quality assured. They include AOT and the angstrom exponent (α), both measured within the wavelength range of 0.340–1.640 μm.

Since the purpose of this study is to investigate the effect of SM and WS variation on coarse-mode dust emission, AOT measurements at 0.5 μm wavelength were used; this is commonly used in characterizing mixed-mode dust particles in the atmosphere. However, AOT at this wavelength is unable to completely reveal the complex nature of particle size distribution and vertical profile of the dust column and should be analysed together with the angstrom exponent (α) to determine the proportions of fine- and coarse-mode dust particles (Eck et al. 1999). The angstrom exponent is defined as the slope of the line plotted between the logarithm of the AOT and the corresponding wavelengths (Angstrom 1929). While there cannot be a sharp threshold value of α for particle size, Eck et al. (2008) have recommended that observations with α (440, 870) values greater than 0.7 are dominated by fine-mode while those with values lower than 0.7 are dominated by coarse-mode desert dust.

Frequency distribution of AERONET AOT over Hamim and Mezaira during the study period (Figure 2(a)) was found to be similar, with a mean AOT of 0.33. This proves that there is no significant difference in dust composition between the two stations, since they are located only 50 km apart. By using a threshold value of 0.7 for α (440, 870), 33% and 40% of the collected observations were identified as fine and coarse mode, respectively. Whereas advection from industrial and urban pollution, and soil, could be the source of fine-mode particles, coarse particles are more likely to be either of local origin generated by the process of saltation and suspension, or transported by strong winds as the soil in the study area and surrounding areas is primarily composed of sand particles (Prospero et al. 2002; Eck et al. 2008; Reid et al. 2008).

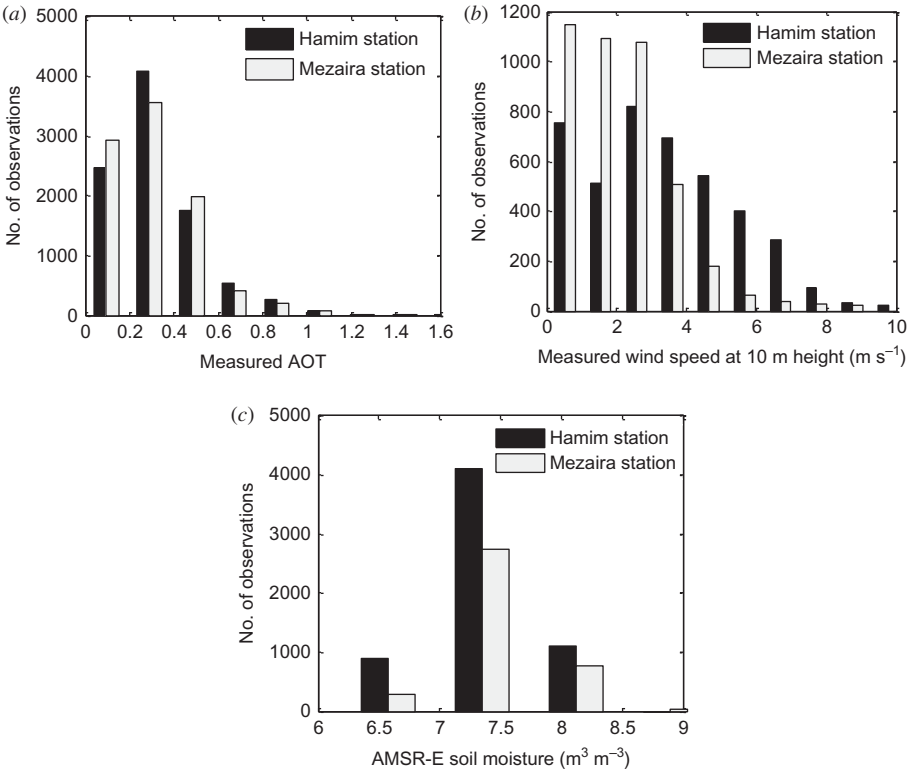

Figure 2. Frequency distribution over Hamim and Mezaira for (*a*) AERONET AOT at 0.5 μm, (*b*) wind speed at 10 m height (m s^{-1}), and (*c*) AMSR-E soil moisture (m^3 m^{-3}).

3.2.2. WS measurements

Hourly WS measurements were collected at 10 m height from two meteorological stations located next to the AERONET stations, with the average hourly WS ranging from 0.1 to 10.6 m s^{-1} (Figure 2(b)). The threshold friction velocity is extremely site specific, but it usually falls within a narrow range in desert regions. For example, threshold friction velocity at 10 m usually ranges between 5 and 9 m s^{-1} in sand-dominated desert regions, but a constant value of 6.5 m s^{-1} was frequently adopted in several dust-modelling studies (Gillette and Passi 1988; Kurosaki and Mikami 2007). In our study, only 7.9% of the WS data exceeded the threshold friction velocity of 6.5 m s^{-1} (Figure 2(b)).

3.2.3. AMSR-E SM data

Daily SM measurements were derived from the passive microwave satellite AMSR-E launched in 2002. This parameter is retrieved from C- or X-band brightness temperature data for the upper 1 cm surface of the soil. AMSR-E measures brightness temperature twice daily, at 01:30 and 13:30 local time, with a spatial resolution of about 0.25° × 0.25° (Njoku et al. 2003). AMSR-E SM data have been widely used and validated in different field campaigns (Owe, de Jau, and Holmes 2008; Wang et al. 2009). Since most dust sources are located in arid or semi-arid regions, it is important to consider the variation and validation of SM in such regions. One such validation study was done by Al-Jassar and Rao (2010), in which AMSR-E-derived SM data were compared by taking one pixel

of AMSR-E data and average gravimetric SM measurements collected over 45 locations (5 cm depth) lying within the pixel over an arid region of Kuwait. Their results showed that AMSR-E-derived SM is in agreement with gravimetric SM data, and the error obtained was within the AMSR-E error range of 3%.

The daily AMSR-E SM measured during the study period ranged between 0.064 and 0.116 $m^3\ m^{-3}$ (Figure 2(*c*)). Unfortunately, the coarse resolution of AMSR-E SM data is the main limitation in this study. However, since we are more interested in the relative changes in SM rather than absolute changes, this would not limit our objective. Furthermore, since the spatial variation of SM is low compared with temporal, it is reasonable to assume that SM is constant over a 25 km × 25 km area.

3.2.4. SEVIRI thermal band data

The MSG/SEVIRI data consist of brightness temperatures $BT_{3.9}$, $BT_{8.7}$, $BT_{10.8}$, and BT_{12}, with a spatial resolution of 3 km and temporal resolution of 15 min. The BTs over the stations are extracted from the pixels nearest to the AERONET measurements. The combination $BTD_{3.9–10.8}$, $BTD_{8.7–10.8,}$ $BTD_{10.8–12}$, and $BT_{3.9}$ considered for this study is based on previous studies undertaken (Ackerman 1989; Zhang et al. 2006; Schepanski et al. 2007). The World Meteorological Organization sand and dust storm warning system (WMO SDSWS) produces RGB composite images using $BTD_{12.0–10.8}$ as red, $BTD_{10.8–8.7}$ as green, and $BT_{10.8}$ as blue for detecting dust over desert during both daytime and nighttime (Martinez, Ruiz, and Cuevas 2009). In the present study, $BT_{10.8}$ was replaced by $BT_{3.9}$ because it showed a slightly higher sensitivity to dust loading over the study area. Besides, since the MSG/SEVIRI BTs are measured at higher wavelengths (3.9, 8.7, 10.8, and 12 μm), they would not be similarly sensitive to AERONET AOT_{500}. In fact, while AERONET instruments measure the optical properties of airborne dust of a size comparable to the wavelength used (0.5 μm), MSG/SEVIRI thermal channels measure the radiative properties of airborne dust of a size comparable to their respective wavelengths. However, this would not limit the purpose of our objective because this study examined the relative effect of SM and WS on AOT, and the BTs/BTDs selected are sensitive to dust loading as demonstrated by Zhang et al. (2006) and Paepe and Dewitte (2009).

In order to assess the sensitivity of these BT/BTDs in dust loading, temporal comparisons were carried out between two reference days in August 2010: one very dusty (5th) and one relatively clear-sky/dust-free (13th). These days were selected from the same month and location (MEZAIRA station) by analysing the AERONET AOT_{500} measurements and high-resolution visible (HRV) images over the study area to ensure similar atmospheric and background conditions. The graphs presented in Figures 3(*a*), (*b*), and (*c*) show temporal variation in BTDs for the two days. As shown in Figure 3(*d*), the AOT_{500} value exceeded 1.0 on 5 August while remaining around 0.4 on 13 August. The results obtained are consistent with the findings of previous studies. While $BTD_{3.9–10.8}$ increased in the presence of dust throughout the day (Figure 3(*a*)), $BTD_{8.7–10.8}$ became less negative compared with clear-sky/dust-free condition (Figure 3(*b*)). Figure 3(*c*) shows clearly that variation in $BTD_{10.8–12}$ can occur in dusty conditions, but it is less than that on a clear-sky/dust-free day. It should be noted that since dust emission is highly variable in time and space, the response of these parameters to the presence of dust may vary under different geographic locations and climatic conditions.

In order to reduce the effect of fine-mode particles on the results obtained, observations in AERONET α (440, 870) values greater than 0.7 were removed from the data set since the WS and SM parameters are directly relevant to coarse-mode desert dust emission, as

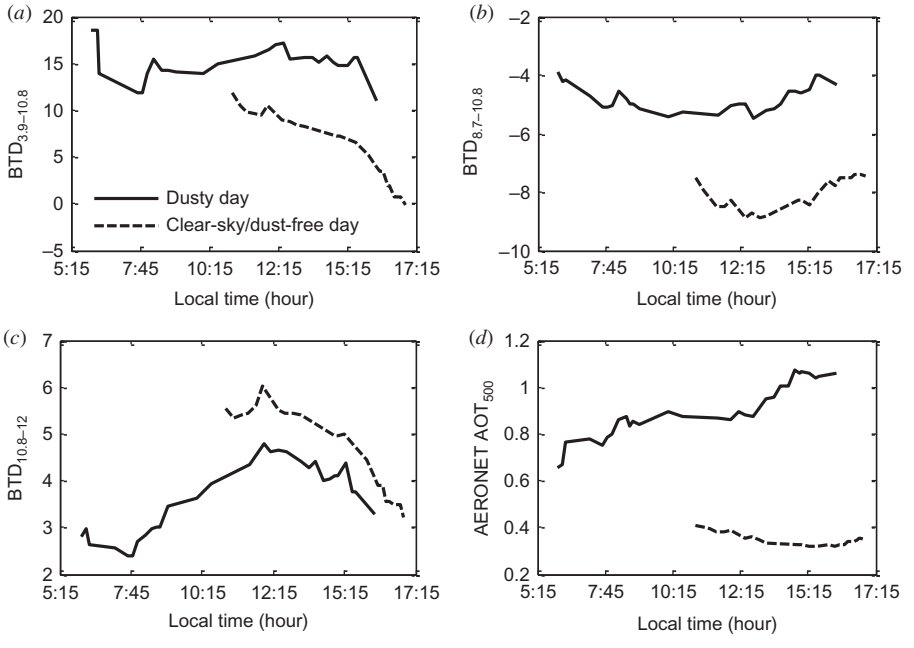

Figure 3. Temporal variation in SEVIRI BTDs and AOT_{500} over Mezaira station on a day of heavy dust (5 August 2010) and a clear-sky/dust-free day (13 August 2010): (*a*) $BTD_{3.9–10.8}$, (*b*) $BTD_{8.7–10.8}$, (*c*) $BTD_{10.8–12}$, and (*d*) AOT_{500}.

discussed by Eck et al. (2008). This filtration reduced the number of observations over the two stations. Since these two stations are in the same area with no significant parametric variations in AERONET AOT_{500} (as discussed in Section 3.2.1), the two data sets were combined to increase the number of data available for analysis and to diversify the training data for better generalization. Finally, a total of 3753 observations corresponding to the coarse mode were extracted over the two stations. Because of the low temporal resolution of SM (2–3 days) and WS (hourly), the effective number of observations available was reduced further. Of the 3753 observations available after filtering (removal of erroneous and missing data), two-thirds (2502) were used for training and one-third (1251) was kept as an independent set for model testing and assessment. A summary of data sets collected for this study is presented in Table 1.

4. Methodology

A neural network-based model was developed to study the effect of SM and WS on coarse-mode dust particle AOT retrieval from the thermal bands of the MSG/SEVIRI satellite. To achieve the specified objectives, the methodology consists of

(1) simulating the base model using the MSG/SEVIRI BT/BTDs combination ($BTD_{3.9–10.8}$, $BTD_{8.7–10.8}$, $BTD_{10.8–12}$, and $BT_{3.9}$) as inputs and AERONET AOT_{500} as output;
(2) adding additional inputs (i.e. SM and WS) one at a time to investigate the contribution of each parameter to the model; and

Table 1. Data set description for Hamim and Mezaira stations (2004–2010).

		Measurements											
		AERONET			MSG/SEVIRI			Wind speed			AMSR-E soil moisture		
Stations	Year	From	To	Number of observations	From	To	Number of observations	From	To	Number of observations	From	To	Number of observations
Hamim	2004	Jun	Dec	9183	Jan	Dec	9183	Jan	Dec	7466	Jan	Dec	6124
	2005	Jan	Aug										
	2006	Jan	Aug										
	2007	Jan	Aug										
Mezaira	2004	Jun	Oct	8318	Jan	Dec	8318	Jan	Dec	4976	Jan	Dec	3842
	2007	Aug	Sep										
	2008	Mar	Nov										
	2009	Nov	Dec										
	2010	Jan	Dec										
	Total			17,501			17,501			12,442			9966
Final data (filtered and coarse mode only)								3753					

(3) applying all inputs (MSG/SEVIRI BT/BTDs combination, SM, and WS) together in the model.

For each combination of inputs (MSG/SEVIRI BT/BTDs, SM, and WS), training and testing were done using two independent data sets. According to accepted procedure, two-thirds of the available data set were used for training and the remaining one-third kept for testing or accuracy assessment. The MBE, RMSE, and R^2 values were calculated for testing the data set of each combination in order to evaluate and compare their influence in estimating AOT_{500}.

The neural network toolbox available in the MATLAB application (Demuth and Beale 1997) was used to develop the ANN model, which was then trained with a feed-forward back-propagation algorithm containing one input layer with the elements of each combination as input nodes, one hidden layer containing the process function, and one output layer for the AOT. The number of nodes in the hidden layer was double that of input nodes. First, the inputs and output were normalized between the interval of [–1 1], then inputs and target output were randomized to avoid errors due to clustering of the data set and to ensure that observations were uniformly distributed in the training and testing data sets. From the training data set, one-third of the data was used for validation. Since the training is unique for each iteration, the results of successive iterations often vary. Therefore, to check the consistency of the model, a simple ensemble network was built by repeating the training process 100 times. In each training step, training and validation data were randomly selected while maintaining their proportions at two-thirds and one-third, respectively. The median of the simulated data was then calculated considering all previous simulation results. For example, a simulated output for the *n*th net would be the median of *n* simulated outputs, where *n* varies from 1 to 100.

Figure 4 shows the typical ANN architecture used in this study when all the inputs are employed for AOT retrieval.

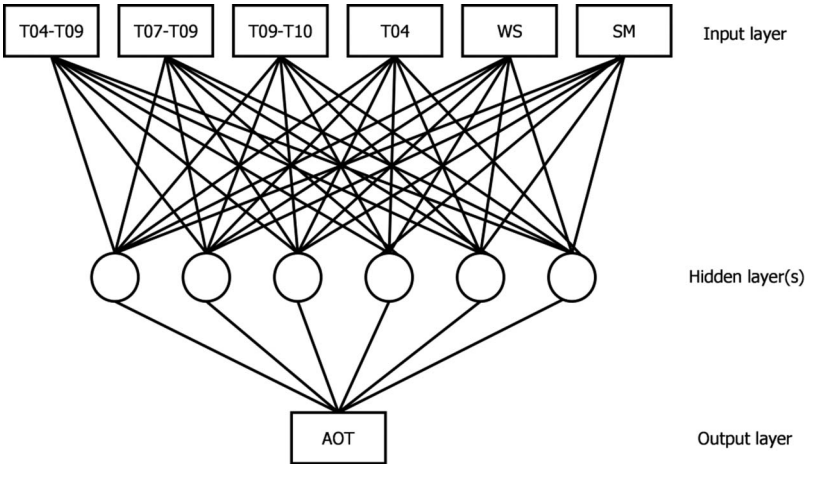

Figure 4. A typical three-layer artificial neural network model as used in this study. The model contains one input layer with '*n*' input neurons, one hidden layer with '2*n*' neurons, and one output layer with one neuron. T04-T09, T07-T09, T09-10, T04, WS, and SM represent $BTD_{3.9–10.8}$, $BTD_{8.7–10.8}$, $BTD_{10.8–12}$, $BT_{3.9}$, wind speed, and soil moisture, respectively.

5. Results and discussion

5.1. SEVIRI thermal band BT/BTDs

The results obtained from the training of our neural network indicate that the suggested combination of SEVIRI inputs ($BT_{3.9–10.8}$, $BT_{8.7–10.8}$, $BT_{10.8–12}$, and $BT_{3.9}$) alone gave a moderate correlation with AERONET AOT_{500} measurements, where an R^2 of 0.68 and an RMSE of 0.114 were obtained (Table 2). This result is in agreement with the findings of similar previous studies (Ackerman 1989; Zhang et al. 2006).

During the training process, the performance of the model and the accuracy of the results obtained were verified by comparing individual and ensemble ANN. The variation in RMSE and MBE is presented in Figures 5(a) and (c). The results obtained show that while RMSE and MBE values fluctuate greatly in individual ANNs, they become stable after about 20 nets. This observation proves that the ensemble ANN is more effective and

Table 2. R^2, MBE, and RMSE obtained for different combinations of inputs.

	Results		
Combinations	R^2	MBE	RMSE
SEVIRI BT/BTDs only	0.68	−0.0008	0.114
SEVIRI BT/BTDs and SM	0.72	−0.0004	0.106
SEVIRI BT/BTDs and WS	0.72	−0.0007	0.107
SEVIRI BT/BTDs, SM, and WS	0.76	−0.0007	0.099

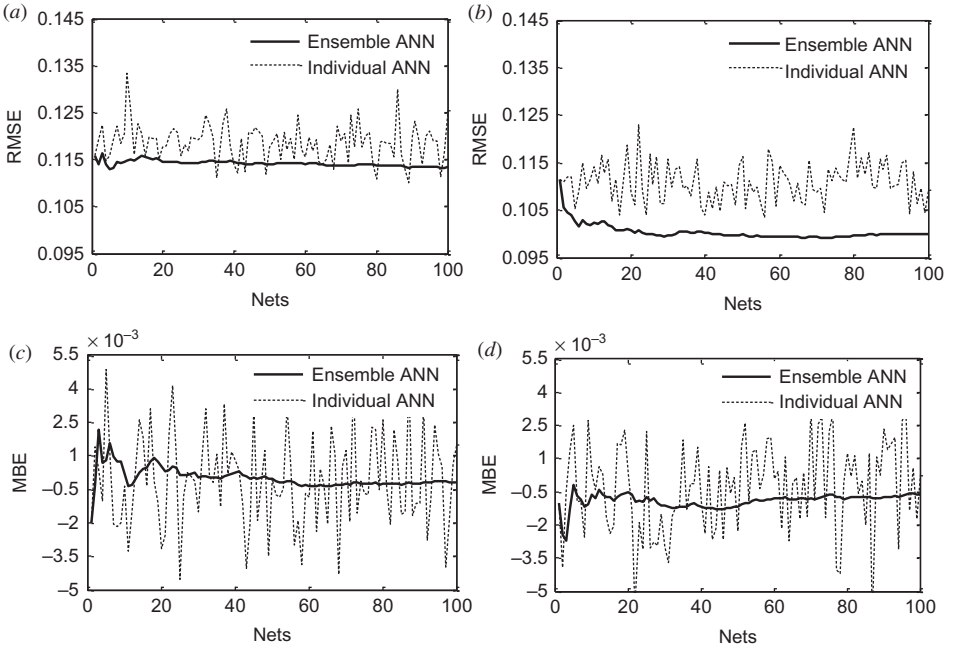

Figure 5. Error of the model in individual and ensemble ANN: (*a*) RMSE for MSG/SEVIRI BT/BTs inputs, (*b*) RMSE for MSG/SEVIRI BT/BTs, SM, and WS inputs, (*c*) MBE for SEVIRI inputs, and (*d*) MBE for SEVIRI, WS, and SM inputs.

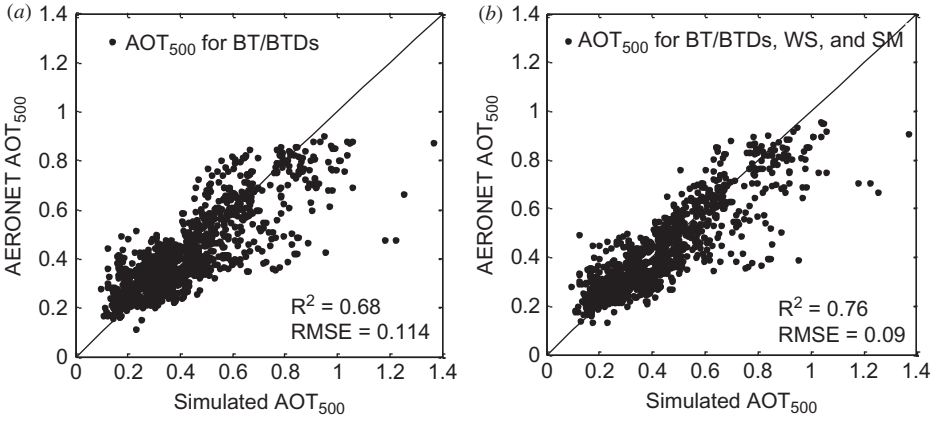

Figure 6. Correlation between simulated and actual AOT for testing data set for the coarse-mode fraction only: (*a*) SEVIRI ($BTD_{3.9–10.8}$, $BTD_{8.7–10.8}$, $BTD_{10.8–12}$, and $BT_{3.9}$) and (*b*) SEVIRI ($BTD_{3.9–10.8}$, $BTD_{8.7–10.8}$, $BTD_{10.8–12}$, and $BT_{3.9}$), SM, and WS.

stable for the purposes of this study. However, ensemble ANN takes longer to train and simulate the model depending on the size of the ensemble.

A scatter plot of AOT_{500} retrieved from SEVIRI BT/BTDs versus measured AERONET AOT_{500} for the testing data set is shown in Figure 6(*a*). It can be seen that the model highly underestimated AOT_{500} values greater than 1. This is because of the limited number of observations in the higher range of AOT_{500} in the training data set, as depicted by the right tail of the histogram in Figure 2(a). For the lower range of values, model performance is satisfactory. Results for the training data set are not presented here due to their inherent bias. Investigation of effects due to change of wavelength in AOT retrieval was also carried out for AOT_{1020} and AOT_{340}. The results for these are not presented here because no significant difference was observed.

5.2. WS and SM effects

In order to analyse the effect of WS and SM on AOT_{500} retrieval, ANN was trained with BT/BTDs, SM, and WS as input data following the process described earlier. As seen in Table 2, the inclusion of SM and WS led to an increase in R^2 from 0.68 to 0.72 and reduced RMSE from 0.114 to 0.10 in each case. The inclusion of WS measured 1 h before AERONET retrieval was also tested for any lag effect, but did not show any significant difference. The corresponding variation in RMSE and MBE is also presented in Figures 5(*b*) and (*d*). Similarly to the previous case, the RMSE and MBE fluctuated markedly in individual ANN but stabilized after a minimum number of nets.

The combined inclusion of SM and WS raised R^2 from 0.68 to 0.76 and lowered RMSE from 0.113 to 0.099. This represents a 5% increase in R^2 and only 1% reduction in RMSE compared with the SEVIRI BT/BTDs single case. Negative MBE, although low in all cases, indicates that the model has a systematic tendency to underestimate AOT (Table 2). A scatter plot of AOT_{500} retrieved from the SEVIRI BT/BTDs, SM, and WS case versus AERONET AOT_{500} measured for the testing data set is shown in Figure 6(*b*). Similar to the previous case, it can be seen that the model underestimated high AOT_{500} values (>1.0) and performed well for the lower range of values.

The result found does not support the commonly used hypothesis that dust emission can be expressed in terms of power of WS, on which several dust emission models such as GOCART (Chin et al. 2000; Ginoux et al. 2001), DEAD (Zender, Bian, and Newman 2003), and GMOD (Yue et al. 2009) are based. This may be because the study area lies in the desert region dominated by sand dunes, which is not a major source of dust. Further, AOT retrieved by the AERONET instrument excludes dust lying outside its field of view, which might be significant depending upon the prevailing WS direction and atmospheric conditions.

The higher R^2 values obtained by adding SM and WS to SEVIRI/MSG BT/BTDs inputs are attributed directly to their effect on the emission of coarse-mode desert dust from the underlying surface. The sandy soil composition in the study area (about 95% sand and 5% clay/silt), coupled with low variation in SM, might have favoured dust emission by saltation. While coarse-mode desert dust generally has a short lifetime of a few hours that prevents its transport to other regions of the globe (Yue et al. 2009), it may still originate from large-scale dust storms such as 'Haboob', as reported by Eck et al. (2008).

The limited contribution of WS and SM to AOT retrieval may be explained in more than one way. Although variation in AMSR-E SM was very low over the study period, as shown in Section 3, it represents the upper 1 cm of soil while sandy soil has a high infiltration rate resulting in moist soil in the deeper layers. It was demonstrated that the upper soil layer may be rapidly eroded during large-scale dust storms because of the drying effect of wind (Bisal and Hsieh 1966), and hence further dust emission would depend on the SM of the underlying soil layer. Also, the data set contains a lower number of observations that exceeds the threshold WS. For a better understanding of the effect of SM and WS on dust emission, this study needs to be expanded to the active sources of dust around the world, such as Bodele in Chad. Owing to the unavailability of WS data, it was not possible to conduct this study in those regions.

6. Conclusion

In this work, the contribution of SM and WS for coarse-mode dust particle retrieval in a desert region over the UAE was evaluated using AERONET AOT_{500} (level 2) measurements. First, a neural network ensemble was created with a combination of SEVIRI BT/BTDs as inputs ($BTD_{3.9–10.8}$, $BTD_{8.7–10.8}$, $BTD_{10.8–12}$, and $BT_{3.9}$). A moderate correlation ($R^2 = 0.68$) was obtained when only BT and BTDs were used as inputs. This result proves a certain correlation between BT/BTDs and AOT_{500}. SM and WS were then applied to the model as additional inputs, and their inclusion increased R^2 from 0.68 to 0.76 and reduced RMSE from 0.113 to 0.09. For more in-depth understanding of dust composition in the atmosphere, a similar model could be developed for AOT at any other wavelength. The relatively low contribution of WS and SM to coarse-mode dust particle AOT retrieval is explained by the complex nature of dust in the UAE, which consists of a mixture of wind-eroded desert dust and long-range dust transported from surrounding areas. In the dust source regions where wind erosion is very active and rainfall is infrequent, the effect of WS and SM on AOT retrieval could be significant. The accuracy of this tool depends strictly on the accuracy of the input parameters and the availability of historical data.

Acknowledgements

The authors would like to extend special thanks to Dr Prashanth Marphu and Dr Saima Munawwar for their valuable feedback. The authors are grateful to the Principal Investigators and their staff from the

AERONET stations at Hamim and Mezaira for their effort in establishing and maintaining the sites. The authors are also grateful to the UAE NCMS for providing the meteorological data. Thanks are also due to the National Snow and Ice Data Centre (NSIDC) for their effort in hosting and maintaining AMSR-E SM data and making them publicly available.

References

Ackerman, S. 1989. "Using the Radiative Temperature Difference at 3.7 and 11 μm to Track Dust Outbreaks." *Remote Sensing of Environment* 27: 129–133.

Ackerman, S. 1997. "Remote Sensing Aerosols Using Satellite Infrared Observations." *Journal of Geophysical Research* 102: 17069–17079.

Al-Jassar, H., and K. Rao. 2010. "Monitoring of Soil Moisture over the Kuwait Desert Using Remote Sensing Technique." *International Journal of Remote Sensing* 31: 4373–4385.

Angstrom, A. 1929. "On the Atmospheric Transmission of Sun Radiation." *Geografiska Annaler* 11: 156–166.

Bagnold, R. 1941. *The Physics of Blown Sand and Desert Dunes*. London: Methuen.

Benediktsson, J., P. Swain, and O. Ersoy. 1990. "Neural Network Approaches Versus Statistical Methods in Classification of Multisource Remote Sensing Data." *IEEE Transactions on Geoscience and Remote Sensing* 28: 540–552.

Bisal, F., and J. Hsieh. 1966. "Influence of Moisture on Erodibility of Soil by Wind." *Soil Science* 102: 43–46.

Boer, B. 1997. "An Introduction to the Climate of the United Arab Emirates." *Journal of Arid Environments* 35: 3–16.

Brindley, H., and J. Russell. 2009. "An Assessment of Saharan Dust Loading and the Corresponding Cloud-Free Longwave Direct Radiative Effect from Geostationary Satellite Observations." *Journal of Geophysical Research* 114: 1–24.

Chepil, W. 1956. "Influence of Moisture on Erodibility of Soil by Wind." *Soil Science* 20: 288–291.

Chin, M., R. Rood, S.-J. Lin, J.-F. Muller, and A. Thompson. 2000. "Atmospheric Sulfur Cycle Simulated in the Global Model GOCART: Model Description and Global Properties." *Journal of Geophysical Research* 105: 24671–24687.

Demuth, H., and M. Beale. 1997. *Neural Network Toolbox User's Guide*. Natick, MA: MathWorks.

EAD. 2009. *Soil Survey of Abu Dhabi Emirate – Volume I Extensive Survey*. Abu Dhabi: EAD.

Eck, T. F., B. N. Holben, J. S. Reid, A. Sinyuk, O. Dubovik, A. Smirnov, D. Giles, N. T. O'Neill, S.-C. Tsay, Q. Ji, A. Al Mandoos, M. Ramzan Khan, E. A. Reid, J. S. Schafer, M. Sorokine, W. Newcomb, and I. Slutsker. 2008. "Spatial and Temporal Variability of Column-Integrated Aerosol Optical Properties in the Southern Arabian Gulf and United Arab Emirates in Summer." *Journal of Geophysical Research* 113: 1–19.

Eck, T., B. Holben, J. Reid, O. Dubovik, A. Smirnov, N. O'Neill, I. Slutsker, and S. Kinne. 1999. "Wavelength Dependence of the Optical Depth of Biomass Burning, Urban and Desert Dust Aerosols." *Journal of Geophysical Research* 104: 31333–31349.

Eissa, Y., M. Chiesa, and H. Ghedira. 2012. "Assessment and Recalibration of the Heliosat-2 Method in Global Horizontal Irradiance Modeling over the Desert Environment of the UAE." *Solar Energy* 86: 1816–1825.

Entekhabi, D., E. Njoku, P. O'Neill, K. H. Kellogg, W. Crow, W. N. Edelstein, J. K. Entin, S. D. Goodman, T. Jackson, J. Johnson, J. S. Kimball, J. R. Piepmeier, R. Koster, N. Martin, K. C. McDonald, M. Moghaddam, S. Moran, R. Reichle, J. C. Shi, M. Spencer, S. W. Thurman, L Tsang, and J. Van Zyl. 2010. "The Soil Moisture Active Passive (SMAP) Mission." *Proceedings of the IEEE* 98: 704–716.

Gillette, D., and R. Passi. 1988. "Modelling Dust Emission Caused by Wind Erosion." *Journal of Geophysical Research* 93: 14233–14242.

Ginoux, P., M. Chin, I. Tegen, J. Prospero, B. Holben, O. Dubovik, and S.-J. Lin. 2001. "Sources and Distributions of Dust Aerosols Simulated with the GOCART Model." *Journal of Geophysical Research* 106: 20255–20273.

Greeley, R., and J. Iversen. 1985. *Wind as Geological Process on Earth, Mars, Venus and Titan*. New York: Cambridge University Press.

Holben, B. N., T. F. Eck, I. Slutsker, D. Tanré, J. P. Buis, A. Setzer, E. Vermote, J. A. Reagan, Y. J. Kaufman, T. Nakajima, F. Lavenu, I. Jankowiak, and A. Smirnov. 1998. "AERONET – A

Federated Instrument Network and Data Archive for Aerosol Characterization." *Remote Sensing of Environment* 66: 1–16.
Hsu, N., S. Tsay, M. King, and J. Herman. 2004. "Aerosol Properties over Bright-Reflecting Source Regions." *IEEE Transactions on Geoscience and Remote Sensing* 42: 557–569.
Jolivet, D., D. Ramon, E. Bernard, P.-Y. Deschamps, J. Riedi, J.-M. Nicolas, and O. Hagolle. 2008. "Aerosol Monitoring Over Land Using MSG/SEVIRI." In *Proceedings of the EUMETSAT Meteorological Satellite Conference*. Darmstadt, Germany: EUMETSAT.
Kellog, C., and Griffin, D. 2006. "Aerobiology and the Global Transport of Desert Dust." *TRENDS in Ecology and Evolution* 21: 638–644.
Kerr, Y., P. Waldteufel, J.-P. Wigneron, J.-M. Martinuzzi, J. Font, and M. Berger. 2001. "Soil Moisture Retrieval from Space: The Soil Moisture and Ocean Salinity (SMOS) Mission." *IEEE Transactions on Geoscience and Remote Sensing* 39: 1729–1735.
Kluser, L., and K. Schepanski. 2009. "Remote Sensing of Mineral Dust over Land with MSG Infrared Channels: A New Bitemporal Mineral Dust Index." *Remote Sensing of Environment* 113: 1853–1867.
Kurosaki, Y., and M. Mikami. 2007. "Threshold Wind Speed for Dust Emission in East Asia and Its Seasonal Variation." *Journal of Geophysical Research* 11: 17202.
Legrand, M., J. Bertrand, M. Desbois, L. Menenger, and Y. Fouquart. 1989. "The Potential of Infrared Satellite Data for the Retrieval of Saharan-Dust Optical Depth over Africa." *Journal of Applied Meteorology* 28: 309–321.
Legrand, M., P. Fattori, and C. N'doume. 2001. "Satellite Detection of Dust Using the IR Imagery of Meteosat 1. Infrared Difference Dust Index." *Journal of Geophysical Research* 106: 18251–18274.
Li, J., P. S. Zhang, J. Schmetz, and W. Menzel. 2007. "Technical Note: Quantitative Monitoring of a Saharan Dust Event with SEVIRI on Meteosat-8." *International Journal of Remote Sensing* 28: 2181–2186.
Marticorena, B., and G. Bergamatti. 1995. "Modeling the Atmospheric Dust Cycle: 1. Design of a Soil-Derived Dust Emission Scheme." *Journal of Geophysical Research* 100: 16415–16430.
Martinez, M., J. Ruiz, and E. Cuevas. 2009. "Use of SEVIRI Images and Derived Products in a WMO Sand and Dust Storm Warning System." *Earth and Environmental Science* 7: 1–6.
Moller, M. 1993. "A Scaled Conjugate Gradient Algorithm for Fast Supervised Learning." *Neural Networks* 6: 525–533.
Njoku, E., T. Jackson, L. Venkataraman, T. Chan, and S. Nghiem. 2003. "Soil Moisture Retrieval from AMSR-E." *IEEE Transactions on Geoscience and Remote Sensing* 41: 215–229.
Owe, M., R. de Jau, and T. Holmes. 2008. "Multisensor Historical Climatology of Satellite-Derived Global Land Surface Moisture." *Journal of Geophysical Research* 113: 1–17.
Paepe, B., and S. Dewitte. 2009. "Dust Aerosol Optical Depth Retrieval over a Desert Surface Using the SEVIRI Window Channels." *Journal of Atmospheric and Oceanic Technology* 26: 704–718.
Paola, J., and R. A. Schowengerdt. 1995. "A Review and Analysis of Backpropagation Neural Networks for Classification of Remotely-Sensed Multi-Spectral Imagery." *International Journal of Remote Sensing* 16: 3033–3058.
Priestley, C. 1959. *Turbulent Transfer in the Lower Atmosphere*. Chicago, IL: University of Chicago Press.
Prospero, J., P. Ginoux, O. Torres, S. Nicholson, and T. Gill. 2002. "Environmental Characterization of Global Sources of Atmospheric Soil Dust Identified with the NIMBUS 7 Total Ozone Mapping Spectrometer (TOMS) Absorbing Aerosol Product." *Reviews of Geophysics* 40: 1–31.
Reid, J., E. Reid, A. Walker, S. Piketh, S. Cliff, A. Mandoos, S. Tsay, and T. Eck. 2008. "Dynamics of Southwest Asian Dust Particle Size Characteristics with Implication for Global Dust Research." *Journal of Geophysical Research* 113: 1–14.
Rumelhart, D., G. Hinton, and R. Williams. 1986. "Learning Representations by Back-Propagating Errors." *Nature* 323: 533–536.
Schepanski, K., I. Tegen, B. Heinold, and A. Macke. 2007. "A New Saharan Dust Source Activation Frequency Map Derived from MSG-SEVIRI IR-Channels." *Journal of Geophysical Research* 34: 1–5.
Selah, A., and D. Fryrear. 1995. "Threshold Wind Velocities of Wet Soils as Affected by Wind Blown Sand." *Soil Science* 60: 304–309.
Shah, S., and F. Palmieri. 1990. "MEKA – A Fast, Local Algorithm for Training Feedforward Neural Networks." In *Proceedings of International Joint Conference on Neural Networks*. San Diego, CA: IJCNN.
Shao, Y. 2008. *Physics and Modelling of Wind Erosion*. Dordrecht: Springer.

Shao, Y., and H. Lu. 2000. "A Simple Expression for Wind Erosion Threshold Friction Velocity." *Journal of Geophysical Research* 105: 22437–22443.

Shenk, W., and R. Curran. 1974. "The Detection of Dust Storms Over Land and Water with Satellite Visible and Infrared Measurements." *Monthly Weather Review* 102: 830–837.

Simmons, A., C. Uppala, D. Dee, and S. Kobayashi. 2007. "ERA-Interim: New ECMWF Reanalysis." *ECMWF Newsletter* 110: 25–35.

Sokolik, I., and O. Toon. 1996. "Direct Radiative Forcing by Anthropogenic Airborne Mineral Aerosols." *Nature* 381: 681–685.

Tso, B., and P. Mather. 2009. *Classification Methods for Remotely Sensed Data*. Boca Raton, FL: CRC Press/Taylor and Francis Group.

Varotsos, C., C. Tzanis, and A. Cracknell. 2009. "The Enhanced Deterioration of the Cultural Heritage Monuments Due to Air Pollution." *Environmental Science and Pollution Research* 16: 590–592.

Wang, L., J. Wen, T. Zhang, Y. Zhao, H. Tian, X. Shi, X. Wang, R. Liu, J. Zhang, and S. Lu. 2009. "Surface Soil Moisture Estimates from AMSR-E Observations over an Arid Area, Northwest China." *Hydrology and Earth System Sciences* 6: 1055–1087.

Wang, Z.-T. 2006. "Influence of Moisture on the Entrainment of Sand by Wind." *Power Technology* 164: 89–93.

Wong, F. 1991. "Time Series Forecasting Using Backpropagation Neural Networks." *Neurocomputing* 2: 147–159.

Yue, X., H. Wang, Z. Wang, and K. Fan. 2009. "Simulation of Dust Aerosol Radiative Feedback Using the Global Transport Model of Dust: 1. Dust Cycle and Validation." *Journal of Geophysical Research* 114: 1–24.

Zender, C., H. Bian, and D. Newman. 2003. "Mineral Dust Entrainment and Deposition (DEAD) Model: Description and 1990s Dust Climatology." *Journal of Geophysical Research* 108: doi: 10.1029/2002JD002775.

Zhang, G., B. Patuwo, and M. Hu. 1998. "Forecasting with Artificial Neural Networks: The State of the Art." *International Journal of Forecasting* 14: 35–62.

Zhang, P., N.-M. Lu, X.-Q. Hu, and C.-h. Dong. 2006. "Identification and Physical Retrieval of Dust Storm Using Three MODIS Thermal IR Channels." *Global and Planetary Change* 52: 197–206.